Mass-Transfer Effects During Separation of Proteins in SMB by Size Exclusion

Joukje Houwing, Hugo A. H. Billiet, and Luuk A. M. van der Wielen
Kluyver Laboratory for Biotechnology, Delft University of Technology, Julianalaan 67, 2628 BC Delft, The Netherlands

The chromatographic fractionation of proteins by size-exclusion chromatography in a simulated moving bed (SMB) is studied. During experimental fractionation of a mixture of bovine serum albumin (BSA) and myoglobin on Sepharose Big Beads, mass-transfer effects are shown to limit the performance of the SMB. The internal profiles, as well as the extract and raffinate compositions, are described well by a steady-state equivalent true moving-bed (TMB) model that incorporates mass-transfer effects. The selection of the particle size in SMB is a trade-off between productivity and mass transfer. Based on the equivalent TMB model, the optimum particle size and configuration of the SMB can be selected, at which preset performance criteria (purity, recovery) are met at specified flow-rate ratios, total column length, and pressure drop. For the current feed and apparatus, an optimal particle size of approximately 145 μm is calculated for achievement of purities and overall recoveries of 95%.

Introduction

In the production of biopharmaceutical proteins, size-exclusion chromatography is a common method of choice as one of the last steps in purification. For example, in the purification of recombinant human serum albumin (*r*HSA), size exclusion is used for removal of dimeric forms as well as degradation fragments of HSA from the monomeric product (Berezenko et al., 1996). Conventional size-exclusion chromatography is a technique of low efficiency, which is predominantly caused by the limited selectivity of the resin material for the target protein or contaminants. To achieve a sufficiently high resolution at the small differences in the distribution coefficients of the solutes to be separated, the ratio of sorbent material to feed volume is large. Only a diluted product can often be obtained. In order to obtain the required purity at a reasonable yield, recycling of product fractions may be needed. This further increases eluent and resin consumption.

Obviously, there is a need for more efficient size-exclusion-based process. Simulated moving-bed (SMB) technology seems an attractive alternative to these troublesome separations. By SMB technology, a continuous feed is fractionated in two (or more) product streams, as is shown in Figure 1. In general, reduced sorbent and solvent needs as compared to fixed-bed chromatography have been reported (Ballanec and Hotier, 1993; Cavoy et al., 1997). Recently, there has been increased interest in the use of SMB technology for the purification of various fine chemicals and biotechnology products. Examples of recent studies include those on the separation of enantiomers (Pais et al., 1997; Cavoy et al., 1997), amino acids (Wu et al., 1998; Van Walsem and Thompson, 1997), and proteins (Houwing et al., 1999; Gottschlich and Kasche, 1997). So far, size-exclusion chromatography in SMB has only been reported for the fractionation of dextran polymers (Ruthven and Ching, 1989), as well as for the desalination of a single protein feed stream (Hashimoto et al., 1988).

A satisfactory performance of the SMB in terms of product purity can only be achieved after proper selection of the liquid and solid flow rates. Methods for selecting the liquid-to-sorbent flow rate ratios usually rely on a local equilibrium approach. In the case of linear adsorption isotherms, the analysis is simple and based on separation factors ($S = \Phi_S K/\Phi_L$) (Ruthven and Ching, 1989). The procedure relies on recognition of the direction of movement of every component in every section required for separation, as is shown in Figure 1. Movement in an upward direction requires a separation factor exceeding unity, whereas downward motion needs separation factors below unity. In the case of nonlinear adsorption isotherms, a more involved analysis based on wave

Correspondence concerning this article should be addressed to L. A. M. van der Wielen.

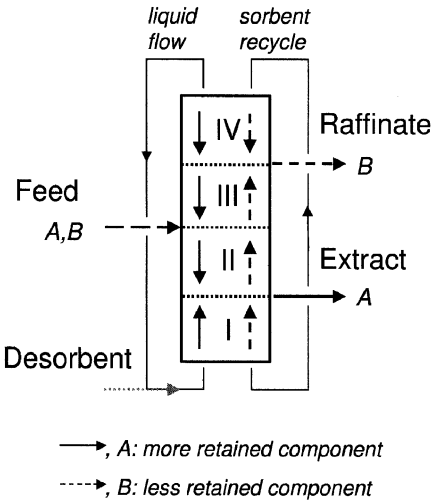

Figure 1. SMB system.

Arrows indicate the direction of movement of components.

theory is usually performed (Storti et al., 1989; Wu et al., 1998). "Triangle theory," the approach of the Morbidelli group (for example, Storti et al., 1993), defines a region of complete separation. Only when the ratios of liquid-to-sorbent flow rates in sections II and III (cf. Figure 1) are chosen inside this region (and provided sections are of sufficient length), a pure extract and a pure raffinate product may be harvested, that is, complete separation can occur. The ratios of the liquid-to-resin flow rates in the various sections of a TMB system, $m = \Phi_L/\Phi_S$, are related to the flow rates Φ^{SMB} and switch time τ in the corresponding SMB system by (Migliorini et al., 1999a)

$$m = \frac{\Phi^{\mathrm{SMB}} \cdot \tau - V\epsilon - V_d}{V(1-\epsilon)} \tag{1}$$

where V is the volume of one column, ϵ is the bed porosity, and V_d is the dead volume per column.

Equilibrium theory thus gives the necessary criteria for design of the SMB. However, these criteria are not sufficient, because mass-transfer and pressure-drop limitations further restrict the operating window. In this study, we focus on the selection of the particle diameter. The optimal particle diameter strikes a balance between productivity, which is limited by the pressure drop, which is in turn favored by large particles, and mass-transfer efficiency, which is favored by small particles. In practice, SMB particle-size selection is often based on prior knowledge of fixed-bed separations. However, this may not result in an optimal particle size for SMB, because of column sizing restrictions in the SMB (Charton and Nicoud, 1995). In order to achieve the required purity and recovery at maximum productivity, it may be useful to use larger particles in the SMB of fixed column length.

The effect of mass-transfer resistances on the performance of the SMB has been shown in several articles. Storti et al. (1989), who based their analysis on dimensionless Stanton numbers, showed that a minimal Stanton number is required to obtain a given separation performance. Zhong and Guiochon (1997), who based the analysis of the effect of mass-transfer resistances on simulations of the simulated moving bed under linear conditions, demonstrated the effect on profiles inside the columns. Wu et al. (1998) showed that mass-transfer effects should be incorporated into the design of an SMB system for separation of amino acid mixtures. In their approach, the mass transfer and dispersion factors are added to the flow-rate ratios obtained from equilibrium analysis. Azevedo and Rodrigues (1999) showed the shrinking of the complete separation region as a function of mass-transfer effects in the case of linear isotherms. The boundaries to the region of complete separation were calculated by repetitively taking an incremental increase in flow-rate ratios, and verifying the complete separation at these settings by numerical simulation. Migliorini et al. (1999b) performed a similar study for isotherms of the bi-Langmuir type, where contours of a given purity were calculated by numerical simulation as a function of the column mass-transfer efficiency.

The optimization of particle size in SMB was described by Charton and Nicoud (1995). The optimal particle size is found at the optimum defined by the maximum overall pressure-drop and the mass-transfer efficiency. In the analysis, it is assumed that the number of columns per section is equal in all sections. For pressure-drop calculations, an average velocity has been taken. This approach is only useful in the case of "symmetric" separations, of components of similar diffusivity, and of feed solutions containing similar concentrations of the two solutes to be separated.

In this study, we have analyzed the optimization of the particle selection for SMB fractionation of a mixture of proteins, where mass-transfer resistances are relatively large. The fractionation of bovine serum albumin (BSA) and myoglobin (myo) has been used as a model separation, and has been studied by both experiment and model. The importance of mass-transfer effects on separation performance is illustrated in experiments in an SMB with a small number of columns, containing relatively large gel particles. In addition, an analysis based on Stanton numbers was performed, in order to select the optimal particle size.

Theory

Fixed-bed and TMB models

The profiles in conventional fixed-bed columns as well as in TMB systems have been simulated numerically. The basis of our models is the one-dimensional (1-D) mass balances for the liquid and sorbent phases

$$\frac{\partial c}{\partial t} = -\upsilon\frac{\partial c}{\partial x} + E\frac{\partial^2 c}{\partial x^2} - \beta \cdot k_o a \cdot (q_{\mathrm{eq}} - q)$$

$$\frac{\partial q}{\partial t} = \upsilon_s\frac{\partial q}{\partial x} + k_o a \cdot (q_{\mathrm{eq}} - q) \tag{2}$$

where c and q are the liquid- and solid-phase concentrations, respectively, and q_{eq} is the solid-phase concentration in equilibrium with c. Only linear equilibria will be considered in this article, hence $q_{\mathrm{eq}} = Kc$, where K is the distribution coefficient. Variables υ and υ_s are the liquid and solid phase interstitial velocities, x is the distance in the column, E is the

axial dispersion coefficient, β is the phase ratio ($(1-\epsilon)/\epsilon$), and $k_o a$ is the overall mass-transfer coefficient. In the case of a conventional fixed-bed column, the solids velocity (v_s) obviously equals zero.

Mass transfer between the two phases is described using a linear driving-force approximation. In order to simplify the set of equations, the axial dispersion term ($E\partial^2 c/\partial x^2$) has been omitted from Eq. 2 and been implemented in the overall mass-transfer coefficient according to Glueckauf (Ruthven, 1984). The definition of the mass-transfer coefficient, as given by Carta and Stringfield (1992), reworked using our notation, is

$$\frac{1}{k_o \cdot a} = \frac{2 d_p K \beta}{v} + \frac{d_p}{6} \cdot \left(\frac{K}{k_L} + \frac{1}{k_S} \right) \tag{3}$$

The first term represents dispersion, the second term represents the mass-transfer resistance in the liquid film surrounding the particle, and the third term represents the mass-transfer resistance in the pore liquid. In this equation, both the left-and righthand sides have been divided by the interfacial area $a = 6/d_p$, where d_p is the particle diameter. The liquid-side mass-transfer coefficient k_L is calculated from dimensionless relations involving the liquid-side Sherwood number (Guiochon et al., 1994)

$$Sh_L = \frac{1.903}{\epsilon} \cdot Re^{0.33} \cdot Sc^{0.33}$$

where

$$Sh_L = \frac{d_p k_L}{D}, \quad Re = \frac{\rho v d_p}{\eta}, \quad \text{and} \quad Sc = \frac{\eta}{D\rho} \tag{4}$$

The diffusion coefficients are assumed to be $D_{BSA} = 6 \cdot 10^{-11}$ m^2/s and $D_{myo} = 10.8 \cdot 10^{-11}$ m^2/s (Laurent and Killander, 1964). Furthermore, η is the viscosity and ρ is the liquid (water) density.

The solid-side mass-transfer coefficient k_S is calculated from the solid-side Sherwood number ($k_S = D_S Sh_S/d_p$) in a similar way. Here Sh_S has been used as a fitting parameter. The intraparticle diffusion coefficient (D_S) was calculated from the free liquid diffusion coefficient (D), the radius of the protein (r_p), and the particle solids fraction (ϕ_f), as was shown by Vonk (1994)

$$\frac{D_S}{D} = \exp\left(- \phi_f^{0.5} \cdot \lambda \right)$$

where

$$\lambda = \frac{r_p}{r_f} \tag{5}$$

The fiber diameter was assumed to be 1.7 nm as described for Sepharose matrices by Vonk (1994). The protein radii were obtained from the Stokes–Einstein relation, which relates the free diffusivity in water to the equivalent solute sphere diameter. For BSA and myoglobin, the calculated radii are 3.64 nm and 1.99 nm, respectively.

In order to calculate the profiles in fixed-bed pulse experiments, the analytical solution of the mass-balance equation (Eq. 2) derived by Carta and Stringfield (1992) is used. This model neglects accumulation in the liquid phase. As suggested by the authors, one column void volume is added to the elution volumes of the peaks in order to be able to account for liquid-phase accumulation.

The steady-state profiles in the equivalent TMB are predicted by an analytical solution of the TMB mass balance equations. The model, which is similar to that of Ruthven and Ching (1989), is shown in the Appendix. The basic equation is the mass balance of the liquid. At steady state, the accumulation in the liquid phase is zero, so the equation reduces to

$$v \cdot \frac{dc}{dx} + \beta k_0 a \cdot (Kc - q) = 0 \tag{6}$$

The relation between the solid- and liquid-phase concentrations is obtained from the overall mass balance over a countercurrent column from the liquid inlet side (position $x = 0$) to position x

$$q - q_0 = \frac{v}{\beta v_s} \cdot (c - c_0) \tag{7}$$

The combination of these two equations results in a differential equation that can be integrated analytically, to yield the profile of one section at known inlet concentrations. When four section balances are combined with the "node-equations," that is, the mass balances over the in- and outlet ports, all concentrations in the equivalent TMB can be calculated.

Optimization of separation performance

The model described in the previous subsection can be used to optimize of the performance of the SMB. The performance is given in terms of purity (P_E and P_R), recovery (R_E, R_R, $R_{\mathrm{ov},A}$ and $R_{\mathrm{ov},B}$, where the latter two indicate the overall recovery of the components in both extract and raffinate) and productivity, the amount of feed processed per unit of system volume (Pr). In this article, the following definitions of these will be used

$$P_E = \frac{c_{A,E}}{c_{A,E} + c_{B,E}} \qquad P_R = \frac{c_{B,R}}{c_{A,R} + c_{B,R}}$$

$$R_E = \frac{(m_2 - m_1) c_{A,E}}{(m_3 - m_2) c_{A,F}} \qquad R_R = \frac{(m_3 - m_4) c_{B,R}}{(m_3 - m_2) c_{B,F}}$$

$$R_{\mathrm{ov},A} = 1 - \frac{m_4 c_{A,W}}{(m_3 - m_2) c_{A,F}} \qquad R_{\mathrm{ov},B} = 1 - \frac{m_4 c_{B,W}}{(m_3 - m_2) c_{B,F}}$$

$$Pr = \frac{\Phi_F}{V_{\mathrm{tot}}} = \frac{(m_3 - m_2) v_s (1 - \epsilon)}{L_{\mathrm{tot}}} \tag{8}$$

In Eq. 8, A is the more retained component, B is the less retained component, and the subscripts E, F, R, and W denote the extract, feed, raffinate, and waste, respectively. The variable L_{tot} represents the added column length.

In the following we will use the TMB model to optimize the purity and recovery as well as the productivity. In this

analysis, it is assumed that the equilibrium- and mass-transfer coefficients do not change when the sorbent particle is increased or reduced in size (Charton and Nicoud, 1995). Furthermore, we will use only TMB situations, that is, where column lengths can have any value and are not restricted to an integer number of columns, such as in the SMB.

Optimization of Purity and Recovery. In the TMB model, only the Stanton numbers influence performance as soon as the flow-rate ratios have been fixed. In order to obtain the system configuration (that is, the lengths of the four sections) that result in a given purity and recovery, the Stanton number needs to be adjusted. This is done conveniently by varying the lengths of the four sections independently in the model, while keeping the variables m, d_p, v_s constant, until the imposed purity and (overall) recovery are met.

Optimization of Productivity. As is clear from Eq. 8, the productivity is determined by the solids interstitial velocity v_s. This velocity is limited by the particle diameter. On the one hand, pressure-drop restrictions only allow a high velocity at large particle diameters. On the other hand, mass-transfer effects only allow a high velocity at small particle diameters. Obviously, there is a trade-off, as is the case in conventional fixed-bed chromatography.

For calculation of the *productivity limited by pressure drop* we assume that the pressure drop per meter limits the flow rate applied in the SMB. The pressure drop per meter under laminar flow conditions is given by the Blake–Kozeny equation

$$\frac{\Delta P}{L} = 170 \frac{\beta^2 \eta v_{\max}}{d_p^2} \tag{9}$$

The maximum productivity with respect to pressure drop is then calculated by combining Eqs. 8 and 9. The relation between $v_{\max}$ and v_s is obtained from Eq. 1. The resulting relation for the maximum productivity determined by the pressure drop, at a known total length, is

$$Pr_{\Delta p} = \left(\frac{(m_3 - m_2)}{\beta m_{\max} + 1 + \frac{V_d}{V\epsilon}} \right) \cdot \frac{\epsilon}{L_{\text{tot}}} \cdot \frac{\frac{\Delta P}{L} \cdot d_p^2}{170 \eta \beta} \tag{10}$$

It is assumed that the ratio of extracolumn dead volume to column volume is constant and independent of the system size.

The calculation of the *productivity limited by mass-transfer effects* is a matter of optimizing the Stanton numbers. In this case, the total column length is imposed, as are the purities and the overall recoveries of the two components (cf. Eq. 8). At fixed values of m and d_p, there are five unknown variables (length of four sections and solids velocity), and five (implicit) equations (two for purity, two for recovery, one for total length). These can be solved using the TMB model. The calculation is repeated for various particle diameters.

As in conventional fixed-bed chromatography, the *optimum particle size* is found by equating the maximum productivity defined by mass-transfer limitations and also defined by pressure-drop limitations.

Experimental

SMB setup

The *laboratory-scale SMB* used in the experiments was built by the Kluyver Laboratory workshop. Four Shimadzu LC8a pumps are used to control the desorbent, extract, feed, and raffinate streams. These pumps are controlled by a Shimadzu LC10a system controller. The positions of the feed and effluent streams in the system are controlled by four twelve-port valves (Valco). Unidirectional flow is established by connecting the recycle stream to open air, similar to Priegnitz (1996). A 24-port valve (Valco) serves this purpose. In our experiments, the liquid waste stream was not recycled to the desorbent stream for further reduction of eluent. Valves were controlled by computer software that was developed in-house.

The *dead volume* connected to each individual column in the SMB system was 0.39 ± 0.01 mL per column. This value is the difference between the residence times of pulses of dextran blue, tryptophan, BSA, and myoglobin on eight separate columns, and the same columns assembled in the SMB. The method for pulse residence time determination is given below.

To monitor the actual flow rates in the SMB system, samples of the extract, raffinate and waste streams were weighed.

Methods

For preparation of the SMB-columns, the matrix was packed in 1-cm-diam Omnifit glass columns at increasing flow rates up to 10 mL/min, resulting in columns of 8.9 cm length, 6.9 mL volume. The beds have a void fraction of 0.39, as was determined by dextran blue pulses. The packing quality of the columns was checked by the pulses of dextran blue (Pharmacia Biotech Benelux) and tryptophan (Merck, Darmstadt). The retention times were 2.70 ± 0.12 mL and 7.87 ± 0.13 mL respectively. A similar procedure was used for preparation of a column for the pulse experiments. Packing was continued up to 6.5 mL/min, resulting in a column of 9.6 cm length.

Single-column pulse experiments were performed on an FPLC system controlled by Unicorn version 2.01 (Amersham Pharmacia Biotech Benelux). Pulses of 100 μL containing 10 g/L protein were injected. Phosphate buffer was used as the eluent. Various flow rates between 0.5 and 4 mL/min were used.

Off-line determinations of the concentrations of the proteins were performed on a PDA spectrophotometer (HP 8435e UV-VIS spectroscopic system, Hewlett-Packard). In addition, the concentrations of the two proteins were monitored by an in-line Shimadzu SPD-M10Avp Photodiode array detector, operated by Class-VP software (version 4.2, Shimadzu).

Using single-component calibration curves, the concentrations of myoglobin and BSA were calculated from the absorption at 405 and 280 nm. The absorption at 405 nm is attributed to myoglobin, since BSA absorption is negligible at that wavelength. From the absorption at 280 nm and the known concentration of myoglobin, the concentration of BSA was calculated.

The *particle void fraction* was determined by weight. The density of a settled bed of particles was determined by weighing a measuring cylinder without (w_m) and with a gel slurry

(w_s), with the slurry volume of water (w_{ws}) and with water of a volume equal to the settled-bed volume (w_{wb}). The settled-bed density ρ_s was calculated from

$$\rho_b = \frac{w_s - w_m - w_{ms} + w_{wb}}{w_{wb} - w_m} \cdot \rho$$

The density of big beads was, thus, determined to be 1,050 kg/m^3. The dry weight of the settled bed (dw_b) was determined in duplicate by drying at 105°C for 2 h. The obtained value, 63.8 g/L, agrees well with the value of the 63.4-g/L bed given by the manufacturer (Kon, personal communication). The fraction of fibers in the sorbent sphere (ϕ_f) was calculated from the preceding data with

$$\rho_b = \epsilon_{sb}\,\rho + (1 - \epsilon_{sb})(1 - \phi_f)\,\rho + dw_b$$

where the porosity of the settled bed was estimated as 0.39. The fraction of fibers obtained in this way was 0.022 mL fiber/mL sorbent sphere.

Materials

An underivatized sepharose big beads matrix, which was a kind gift from Amersham Pharmacia Biotech Benelux, was used. This matrix, with an average particle diameter of 200 μm, is made of highly cross-linked agarose.

In all experiments, a 10-mM phosphate buffer, pH 7, containing 0.1 M NaCl was used as eluent. In the SMB experiments, a feed solution containing 1 g/L myoglobin from horse heart (Sigma cat. no. M1882, $>90\%$ pure) and 5 g/L BSA (Sigma, cat. no. A7906) were used.

Results

Pulse experiments

Both the position and the shape of the response to pulse experiments were a strong function of the applied liquid velocity (see Figure 2 for BSA experiments). This supports the hypothesis that mass-transfer resistances play an important role in the size exclusion of proteins on such large diameter particles and at high liquid velocities. Best fits of the analytical solution to the chromatograms were obtained when $K_{\text{myo}} = 0.88$, $K_{\text{BSA}} = 0.65$, and $Sh_s = 6.64$. The best fits have been determined by the sum of the sum of squared errors (SSE) ($= \Sigma(c_{\text{measured}} - c_{\text{model}})^2$) of all experiments. Figure 2 shows a comparison of the normalized experimental chromatograms and model predictions at a flow rate of 1 mL/min as an example. At higher flow rates, the accuracy of the prediction decreased; the SSE increased from 0.003 at a liquid flow rate of 1 mL/min to 0.09 at a liquid flow rate of 4 mL/min. At the high flow rates, the mass-transfer effects were overpredicted by the model.

SMB experiments

In neither of the five SMB experiments, the conditions of which are shown in Table 1 and Figure 3, 100% purity of either of the two products was obtained (cf. Table 1). Complete separation was expected in experiments II, III, and IV, as these experiments were chosen well inside the "triangle of complete separation," as is shown in Figure 3. This clearly reflects the effects of mass-transfer limitations. Large mass-transfer resistances result in broadening of the fronts between the loaded and unloaded parts of the column. Hence, the end of the BSA desorptive front can extend beyond the extract outlet and result in BSA contaminating the extract

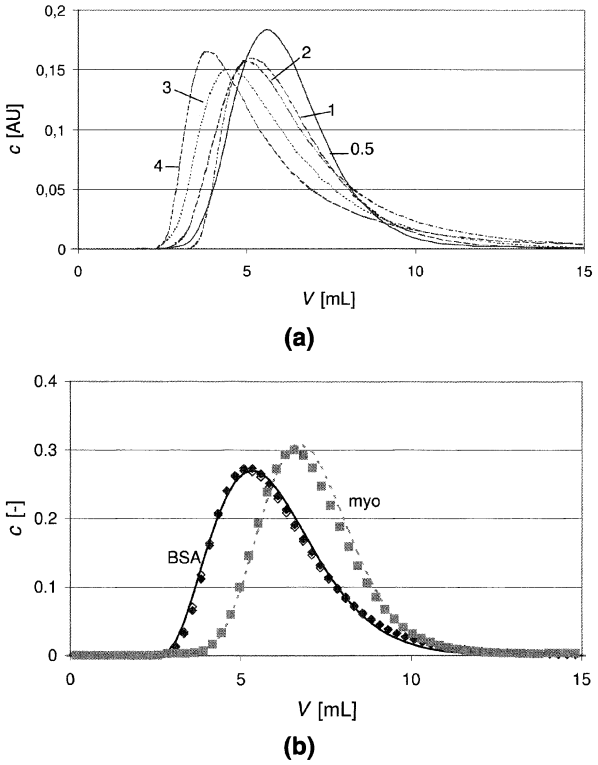

Figure 2. (a) Variations in experimental peak shape of pulses of BSA at different liquid velocities. Numbers indicate flow rates in mL/min; (b) example of simulated pulse chromatograms at 1 mL/min calculated from analytical solution (Parameters used in simulation: $K_{\text{BSA}} = 0.67$; $K_{\text{myo}} = 0.85$; $Shs = 8$).

Table 1. Experimental Conditions, Outlet Concentrations, and Calculated Purities.

Experiment	I	II	III	IV	V
m_1	1.02	1.02	1.02	1.02	1.02
m_2	0.62	0.66	0.72	0.78	0.84
m_3	0.66	0.70	0.76	0.82	0.88
m_4	0.33	0.31	0.30	0.31	0.31
c_{myo} extract [g/L]	0.09	0.10	0.11	0.10	0.09
c_{BSA} extract [g/L]	0.22	0.17	0.12	0.10	0.07
c_{myo} raffinate [g/L]	0.00	0.01	0.01	0.02	0.04
c_{BSA} raffinate [g/L]	0.28	0.31	0.31	0.34	0.35
c_{myo} waste [g/L]	0.00	0.00	0.00	0.00	0.00
c_{BSA} waste [g/L]	0.01	0.01	0.00	0.01	0.01
Purity extract	0.30	0.38	0.47	0.50	0.54
Purity raffinate	0.99	0.98	0.96	0.94	0.90

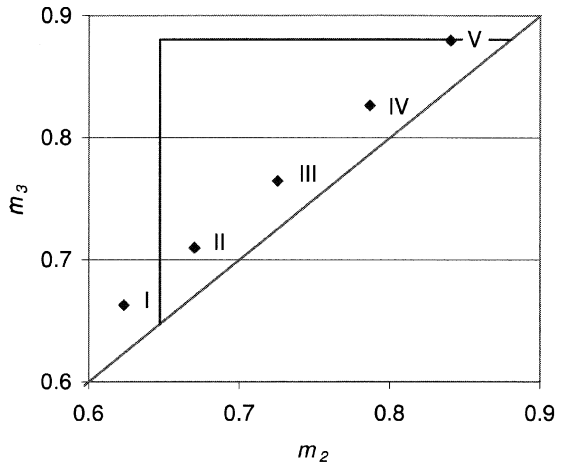

Figure 3. Position of experimental points (♦) relative to the region of complete separation for myoglobin and BSA.

Roman numbers refer to experiment numbers in Table 1.

stream. This is seen in Figure 4, which compares the measured concentrations leaving each column at half the cycle time (Ruthven and Ching, 1989) and the model predictions of the profile for experiment III.

Even though the harvested products are not pure, enrichment does occur. This is illustrated by the concentration ratio of BSA to myoglobin. The feed solution contained 5 g/L BSA and 1 g/L myoglobin, a BSA to myoglobin ratio of 5. The extract is enriched in myoglobin, as shown by a decrease in this ratio to 1 in Figure 4. The raffinate is enriched in BSA, as shown by an increase of the ratio to 40.

The tendencies between variation in flow-rate ratios and separation performance of the mass-transfer-limited size-exclusion SMB agreed qualitatively with the expected SMB behavior. For instance, a simultaneous increase in the flow-rate ratio in sections II and III results in the increased recovery of both components in the raffinate product and the decreased recovery of both proteins in the extract product. This is expected, since the upward transport of both BSA and myoglobin is favored by an increasing flow rate. The quantitative

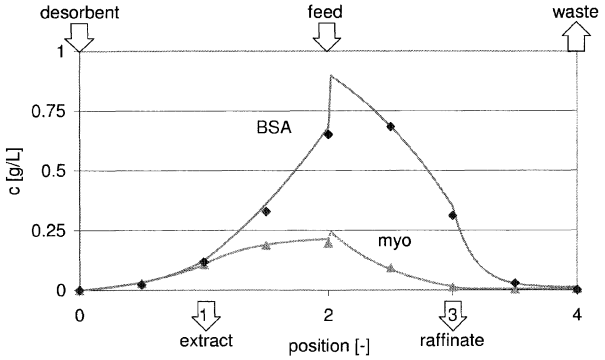

Figure 4. Experimental (symbols) and simulated (lines) concentration profiles along the laboratory-scale SMB in experiment III.

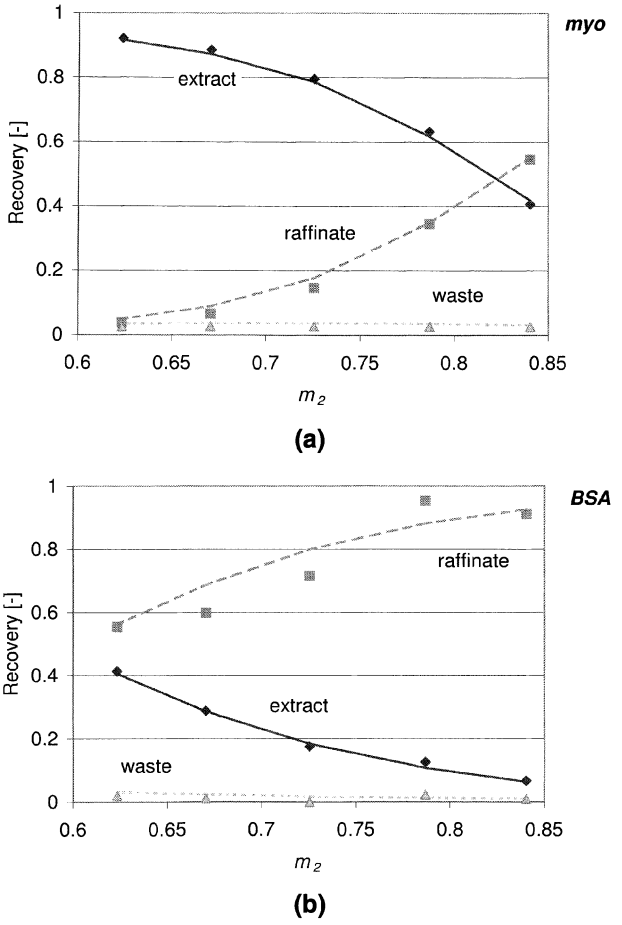

Figure 5. Recovery of myoglobin (a) and BSA (b) in extract, raffinate, and waste streams.

Symbols represent experimental values, lines indicate model predictions.

agreement between experimental and predicted performance is good, as can be seen in Figure 5, which shows a comparison of the predicted and experimental recoveries as calculated from on-line analysis at steady state in the five experiments as a function of m_2.

Optimization of purity and recovery

Obviously, the experimental Stanton numbers have been too low to attain complete separation. The Stanton numbers that are required to obtain a given purity and recovery were calculated using the TMB model. Arbitrarily, the extract and raffinate purity and overall recovery of both BSA and myoglobin have been chosen at 95%. The particle diameter and solids interstitial velocity were kept constant at the experimental values of 200 μm and 0.0013 m/s, respectively. At these constant values, only the column lengths per section determine the Stanton number; hence, in Figure 6 we only represented the section lengths calculated per experiment. This figure lacks data on experiment I, as this point has been chosen too far outside the region of complete separation to obtain the given purity and recovery using any combination

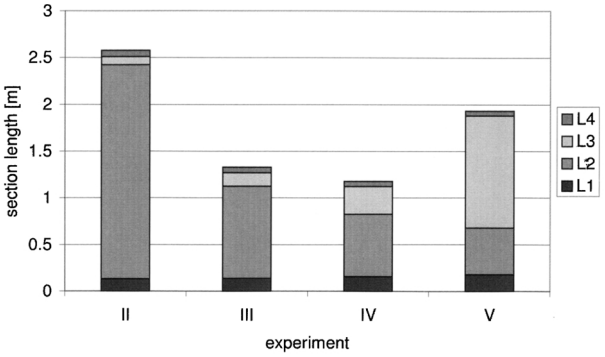

Figure 6. Optimal column length for achieving $P_E = P_R = R_{ov}, A = R_{ov}, B = 95\%$, $dD_p = 200$ μm, $v_s = 0.0013$ m/s.

of column lengths. In this case, equilibrium (rather than mass transfer) prohibits the attainment of complete separation.

The figure shows that a rather short section I and IV will suffice in all experiments. This agrees with the choice of the operating point, which is rather far from the respective boundaries. Sections II and III require more length. It is seen that, traveling from experiment II to experiment V, the calculated required length of section II is decreased and the length of section III is increased. This is expected, as the operating points drift away from the m_2-boundary and increasingly approach the m_3-boundary. The total length is minimal in experiment IV. This operation is well inside the triangle, closer to the m_3-boundary than to the m_2-boundary. This asymmetry reflects the asymmetric feed concentrations chosen; the change in concentration of BSA, with a feed concentration of 5 g/L, is much higher than that of myoglobin, with a feed concentration of 1 g/L.

Note that the analysis per section is not included in the procedure described by Charton and Nicoud (1995). This might lead to an unnecessarily high efficiency in sections I, III, and IV, or one that is too low in section II.

Optimization of productivity

For optimization of productivity as a function of the particle diameter, the system variables (total column length and maximum pressure drop), as well as the performance parameters, are set at a chosen value. In practice, these are enforced by the available SMB system, or the requirements on the products. Essentially, this is an economic optimization. In this article, we only optimized productivity as such, as the economic optimization contains many (company) specific figures. In this subsection, we give the results of optimization of the particle size with variable system length (Figure 7A), with variable maximum allowed pressure drop per meter (Figure 7B), and with variable separation performance (Figure 7C). This is done in order to sketch the variance in the optimal particle size. The m-values of experiment III were used in all

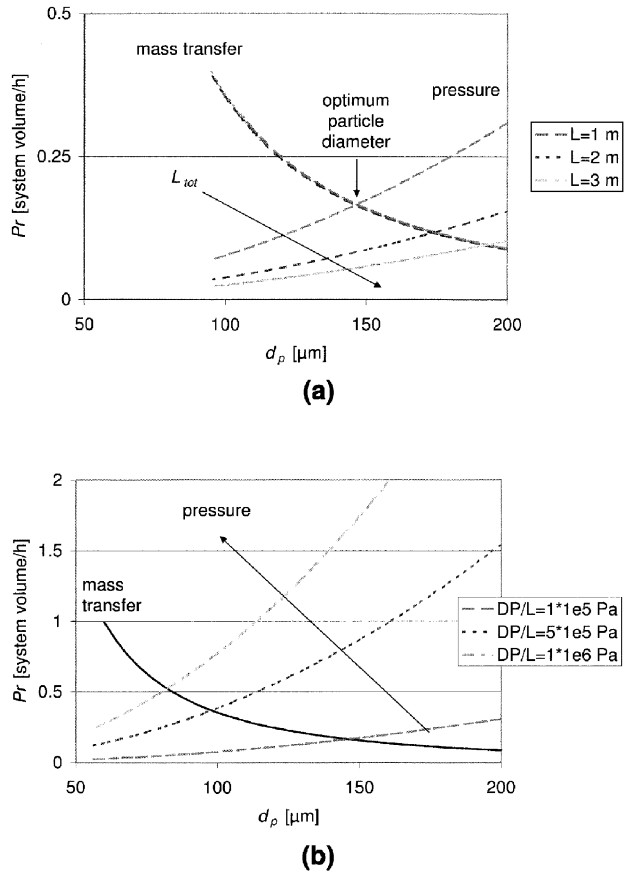

Figure 7. Optimization of productivity as a function of particle size at conditions of experiment III.

(a) Effect of total length; (b) effect of pressure drop; (c) effect of purity and recovery requirements.

calculations. The base case is the situation with a total system length of 1 m, a pressure drop of 10^5 Pa/m, and $P_E = P_R = R_{ov,A} = R_{ov,B} = 95\%$. In the base case, the optimum particle diameter equals 145 μm, which is indeed much smaller than the experimental 200 μm. In the base case, the optimal distribution of column length per section $L_1{:}L_2{:}L_3{:}L_4$ is 1.05:7.42:1.09:0.45. These figures did not change very much in comparison to the values shown in Figure 6 upon changing the particle diameter. This is due to the fact that the resistance to mass transfer is predominantly in the solid phase; the third term in Eq. 3 is approximately 50 times as large as the first and second term. Hence, the Stanton number is proportional to $L/(v_s \cdot d_p^2)$. Constant Stanton numbers (required for a constant separation performance) are achieved when v_s is proportional to d_p^2, without changing the length per section.

When the total system length is varied, the productivity determined by mass transfer is almost invariable. Again this is a result of the mass-transfer resistance being predominantly at the solids side of the particle. The Stanton number is then constant when the ratio L/v_s is constant. According to Eq. 8, productivity is then also constant. The productivity as limited by the pressure drop depends on the system length, as suggested by Eq. 10. The combination of the two effects is that the optimum particle size shifts to increased values upon increasing the system length.

When the maximum allowed pressure drop is increased, the optimum particle size is shifted to smaller particles, for obvious reasons.

The change in the purity requirements to lower values leads to a shift in the optimum particle size to larger particles. This is expected, as lower Stanton values are sufficient to reach the given performance.

Conclusions

SMB systems can be used for the fractionation of two proteins by size-exclusion chromatography. In experiments with an aqueous feed stream containing BSA and myoglobin, the obtained extract streams were enriched in myoglobin and the raffinate streams were enriched in BSA. Equilibrium theory has been used to define the conditions for complete separation (triangle theory), but no complete separation has been observed. Clearly, this is due to slow mass transfer of macromolecules, such as proteins in porous matrices. The experimental concentration profiles agree well with those calculated with a steady-state true moving-bed model, using a linear driving-force approximation for the mass-transfer description.

SMB systems, optimized with respect to productivity per resin volume per time and eluent consumption, and operate under a mass-transfer limitation. This should be taken into account when defining the proper operating conditions. There are minimum values for the Stanton numbers required to obtain a given purity and recovery in each of the sections of an SMB system. These minimum Stanton numbers can be identified using an equivalent TMB model, after selection of the purity of the extract and raffinate product and the overall recovery of the two proteins. Column length per section, liquid velocity, and particle size can be selected in such a way that these criteria are met for Stanton numbers.

The productivity at the m-values of experiment III has been optimized with respect to particle diameter. In the "base case," where the total length equals 1 m, the maximum pressure drop is 10^5 Pa/m and $P_E = P_R = R_{ov,A} = R_{ov,B} = 95\%$, the optimum particle size is 145 μm, and the distribution of column lengths $L_1{:}L_2{:}L_3{:}L_4$ is 1.05:7.42:1.09:0.45. The optimum particle diameter shifts to smaller particle size as the pressure drop is increased, purity and recovery requirements are increased, or the total column length is decreased. These figures show that the equivalent TMB model can well be used for optimization of performance criteria. It should be noted that in practical systems, the optimization is an economical one; however, by changing the objective function, the TMB model can also be used for that purpose.

Acknowledgments

The Dutch Ministry of Economic Affairs is gratefully acknowledged for the financial support in the framework of the IOP Milieutechnologie (Preventie) program. Amersham Pharmacia Biotech is acknowledged for the gift of gel materials.

Notation

A = column area, m^2
a = solid–liquid interfacial area, L/m
c = liquid-phase concentration, g/L
D = diffusion coefficient, m^2/s
D_p = effective diffusion coefficient in sorbent pores, m^2/s
d_p = particle diameter, m
E = dispersion coefficient, m^2/s
K = distribution coefficient
k_o = overall mass-transfer coefficient, m/s
L = column length, m
L_s = section length, m
m = flow-rate ratio $[\Phi_L/\Phi_S]$
Pe = Peclet number $[vL/E]$
Pr = productivity, system volume/h
q = solid-phase concentration, g/L
r_f = fiber radius, nm
r_p = Stokes radius of protein, nm
S = Separation factor $[\Phi_S K/\Phi_L]$
Sc = Schmidt number $[\eta/D\rho]$
St = Stanton number $[k_o a L_s/v_s]$
t = time, s
u = superficial velocity, m/s
v = interstitial velocity, m/s
v_s = solid-phase interstitial velocity, m/s
V = column volume, m^3
V_d = dead volume per column, m^3
V_{tot} = total system volume, m^3
x = distance, m
z = dimensionless distance $[x/L]$

Greek letters

β = phase ratio $[(1-\epsilon)/\epsilon]$
ϵ = porosity
ϕ_f = particle solids fraction
λ = aspect ratio
η = viscosity, Pa·s
ρ = density, kg/m^3
θ = dimensionless time
τ = switch time, s
Φ = volumetric flow rate, m^3/s

Literature Cited

Azevedo, D. C. S., and A. E. Rodrigues, "Design of a Simulated Moving Bed in the Presence of Mass-Transfer Resistances," *AIChE J.*, **45**, 956 (1999).

Ballanec, B., and G. Hotier, "From Batch to Simulated Countercurrent Chromatography," *Preparative and Production Scale Chromatography*, G. Ganetsos and P. E. Barker, eds., Dekker, New York (1993).
Berezenko, S., A. V. Quirk, P. C. Wood, J. R. Woodrow, D. Sleep, H. van Urk, S. J. Burton, J. Stephen, A. R. Goodey, and R. A. Johnson, "Process of High Purity Albumin Production," World Patent Application No. WO 9,637,515 (1996).
Cavoy, E., M.-F. Deltent, S. Lehoucq, and D. Miggiano, "Laboratory-Developed Simulated Moving Bed for Chiral Drug Separations. Design of the System and Separation of Tramadol Enantiomers," *J. Chromatog.*, **769**, 49 (1997).
Carta, G., and W. B. Stringfield, "Analytic Solution for Volume-Overloaded Gradient Elution Chromatography," *J. Chromatog.*, **605**, 151 (1992).
Charton, F., and R. Nicoud, "Complete Design of a Simulated Moving Bed," *J. Chromatog.*, **702**, 97 (1995).
Gottschlich, N., and V. Kasche, "Purification of Monoclonal Antibodies by Simulated Moving Bed Chromatography," *J. Chromatog.*, **765**, 201 (1997).
Guiochon, G., S. Golshan-Shirazi, and A. M. Katti, *Fundamentals of Preparative and Nonlinear Chromatography*, Academic Press, Boston (1994).
Hashimoto, K., S. Adachi, and Y. Shirai, "Continuous Desalting of Proteins with a Simulated Moving Bed Adsorber," *Agric. Biol. Chem.*, **52**, 2161 (1988).
Houwing, J., H. A. H. Billiet, J. A. Wesselingh, and L. A. M. van der Wielen, "Azeotropic Phenomena During Separation of Dilute Mixtures of Proteins by Simulated Moving Bed Chromatography," *J. Chem. Technol. Biotechnol.*, **74**, 213 (1999).
Laurent, T. C., and J. Killander, "A Theory of Gel Filtration and Its Experimental Verification," *J. Chromatog.*, **14**, 317 (1964).
Migliorini, C., M. Mazzotti, and M. Morbidelli, "Simulated Moving Bed Units with Extra-Column Dead Volume," *AIChE J.*, **45**, 1411 (1999a).
Migliorini, C., A. Gentilini, M. Mazzotti, and M. Morbidelli, "Design of Simulated Moving Bed Units Under Nonideal Conditions," *Ind. Eng. Chem. Res.*, **38**, 2400 (1999b).
Pais, L. S., J. M. Loureiro, and A. Rodrigues, "Separation of 1,1-bi-2-Naphthol Enantiomers by Continuous Chromatography in Simulated Moving Bed," *Chem. Eng. Sci.*, **52**, 245 (1997).
Priegnitz, J. W., "Small Scale Simulated Moving Bed Separation Process," U.S. Patent No. 5,565,104 (1996).
Ruthven, D. M., *Adsorption and Adsorption Processes*, Wiley, New York (1984).
Ruthven, D. M., and C. B. Ching, "Countercurrent and Simulated Countercurrent Adsorption Separation Processes," *Chem. Eng. Sci.*, **44**, 1011 (1989).
Storti, G., M. Masi, S. Carrà, and M. Morbidelli, "Optimal Design of Multicomponent Countercurrent Adsorption Separation Processes Involving Nonlinear Equilibria," *Chem. Eng. Sci.*, **44**, 1329 (1989).
Storti, G., M. Mazzotti, M. Morbidelli, and S. Carrà, "Robust Design of Binary Countercurrent Adsorption Separation Processes," *AIChE J.*, **39**, 471 (1993).
Vonk, P., *Diffusion of Large Molecules in Porous Structures*, PhD Thesis, Groningen State Univ., Groningen, The Netherlands (1994).
Van Walsem, H. J., and M. C. Thompson, "Simulated Moving Bed in the Production of Lysine," *J. Biotechnol.*, **59**, 127 (1997).
Wu, D.-J., Y. Xie, and N. H. L. Wang, "Design of Simulated Moving Bed Chromatography for Amino Acid Separations," *Ind. Eng. Chem. Res.*, **37**, 4023 (1998).
Zhong, G., and G. Guiochon, "Simulated Moving Bed Chromatography. Effects of Axial Dispersion and Mass Transfer Under Linear Conditions," *Chem. Eng. Sci.*, **52**, 3117 (1997).

Appendix: Steady-State TMB Model

In the case of linear equilibria, the profiles in a true moving bed at steady state can be calculated analytically (cf. Ruthven and Ching, 1989). Let us consider one section of the true moving bed. Since the TMB is at steady state, all accumulation terms cease. When axial dispersion is integrated in the (linear driving force) mass-transfer term, such as in Eq. 3, the mass balance over the liquid phase at position x in the section reduces to

$$\upsilon \cdot \frac{dc}{dx} + \frac{1-\epsilon}{\epsilon} \cdot k_o a \cdot (Kc - q) = 0 \tag{A1}$$

In our calculations, the mass-transfer coefficient is related to the SMB interstitial velocities. The solid- and liquid-phase concentrations can be related via a balance relating the concentrations c and q at position x to the concentrations c_0 and q_0 at the liquid inlet side of the section (that is, the bottom; position $x = 0$)

$$q - q_0 = \frac{\epsilon}{1-\epsilon} \frac{\upsilon}{\upsilon_s} \cdot (c - c_0) \tag{A2}$$

After substituting Eq. A2 in Eq. A1 and introducing the dimensionless variables, $St = k_o a L_s/\upsilon_s$ and $z = x/L_s$, and the separation factor, S, defined as $S = K\beta\upsilon_s/\upsilon$, the mass-balance equation can be rewritten in a dimensionless form

$$\frac{dc}{dz} = -St \cdot \left[(S-1)c + c_0 - \frac{Sq_0}{K} \right] \tag{A3}$$

This equation can be integrated analytically, yielding an equation containing only concentration (c) and location (z) and the concentrations at the bottom of the section (q_0,c_0)

$$\frac{(S-1)c + c_0 - \dfrac{Sq_0}{K}}{(S-1)c_0 + c_0 - \dfrac{Sq_0}{K}} = \exp\left[St(1-S)z \right] \tag{A4}$$

A similar mass balance can be written for all four sections of the TMB.

The bottom concentrations can be obtained from the mass balances relations at points of mixing of streams, the "nodes." These are

$$\begin{aligned}
q_0^{\mathrm{I}} &= q_L^{\mathrm{IV}} \qquad & c_0^{\mathrm{I}} &= c^D \\
q_0^{\mathrm{II}} &= q_L^{\mathrm{I}} \qquad & c_0^{\mathrm{II}} &= c_L^{\mathrm{I}} \\
q_0^{\mathrm{III}} &= q_L^{\mathrm{II}} \qquad & c_0^{\mathrm{III}} &= \frac{m_2}{m_3} c_L^{\mathrm{II}} + \left(\frac{m_3 - m_2}{m_3} \right) c^F \\
q_0^{\mathrm{IV}} &= q_L^{\mathrm{III}} \qquad & c_0^{\mathrm{IV}} &= c_L^{\mathrm{III}}
\end{aligned} \tag{A5}$$

Simulation of a TMB profile can then be done in two steps. The first step is to find the ten node concentrations (c_0^{I}, c_0^{II}, c_0^{III}, c_0^{IV}, c_L^{IV}, q_0^{I}, q_0^{II}, q_0^{III}, q_0^{IV}, q_L^{IV}). This is done by combining the mass balance (Eq. A2) from the bottom ($x = 0$) to the top ($x = L$) of the section with the node equations (Eq. A5), for example, for section I

$$q_0^{\mathrm{II}} = q_L^{\mathrm{I}} = q_0^{\mathrm{I}} + m_1\left(c_L^{\mathrm{I}} - c_0^{\mathrm{I}}\right) = q_0^{\mathrm{I}} + m_1\left(c_0^{\mathrm{II}} - c_0^{\mathrm{I}}\right) \tag{A6}$$

The relation between c_0 and c_L is obtained from integration of the liquid balance (Eq. A4) to $z = 1$. For convenience, the latter is rewritten using two dummy variables, f and g

$$(S-1)c_L = c_0 f + q_0 g$$

where

$f = S\exp\left[St\cdot(1-S)\right]-1$ and

$$g = \frac{S}{K}\left\{1-\exp\left[St\cdot(1-S)\right]\right\} \quad \text{(A7)}$$

combining four equations like Eq. A4 and four like Eq. A6 and the node balance over the desorbent inlet results in a set of 10 equations, which is, written in matrix form

$$\begin{bmatrix} f_1 & g_1 & 1-S^{\mathrm{I}} & 0 & 0 & 0 & 0 & 0 & 0 & 0 \\ m_1 & -1 & -m_1 & 1 & 0 & 0 & 0 & 0 & 0 & 0 \\ 0 & 0 & f_2 & g_2 & 1-S^{\mathrm{II}} & 0 & 0 & 0 & 0 & 0 \\ 0 & 0 & m_2 & -1 & -m_2 & 1 & 0 & 0 & 0 & 0 \\ 0 & 0 & 0 & 0 & f_3 h_1 & g_3 & 1-S^{\mathrm{III}} & 0 & 0 & 0 \\ 0 & 0 & 0 & 0 & m_3 h_1 & -1 & -m_3 & 1 & 0 & 0 \\ 0 & 0 & 0 & 0 & 0 & 0 & f_4 & g_4 & 1-S^{\mathrm{IV}} & 0 \\ 0 & 0 & 0 & 0 & 0 & 0 & m_4 & -1 & -m_4 & 1 \\ m_1 & 0 & 0 & 0 & 0 & 0 & 0 & 0 & 0 & 0 \\ 0 & 1 & 0 & 0 & 0 & 0 & 0 & 0 & 0 & -1 \end{bmatrix} \cdot \begin{bmatrix} c_0^{\mathrm{I}} \\ q_0^{\mathrm{I}} \\ c_0^{\mathrm{II}} \\ q_0^{\mathrm{II}} \\ c_0^{\mathrm{III}} \\ q_0^{\mathrm{III}} \\ c_0^{\mathrm{IV}} \\ q_0^{\mathrm{IV}} \\ c_L^{\mathrm{IV}} \\ q_L^{\mathrm{IV}} \end{bmatrix} = \begin{bmatrix} 0 \\ 0 \\ 0 \\ 0 \\ -f_3 h_2 \\ -m_3 h_2 \\ 0 \\ 0 \\ 0 \\ 0 \end{bmatrix} \quad \text{(A8)}$$

where $h_1 = m_2/m_3$ and $h_2 = (m_3 - m_2)/m_3$. Note that the separation factors and the Stanton numbers vary from section to section. After solving this set of equations by matrix inversion (for instance, using commercial software such as Mathcad (MathSoft Corp.), the node concentrations are known.

The second step in calculating the profile over the TMB is to calculate the concentrations at various positions (z) in the sections via Eq. A4, where the node concentrations are used for c_0 and q_0. Thus, the procedure is completed.

Manuscript received Apr. 2, 2001, and revision received Sept. 24, 2002.